STEM CELLS®

REGENERATIVE MEDICINE

Passive Stretch Induces Structural and Functional Maturation of Engineered Heart Muscle as Predicted by Computational Modeling

OSCAR J. ABILEZ,[a,b,c,d*] EVANGELINE TZATZALOS,[a,b*] HUAXIAO YANG,[a,b] MING-TAO ZHAO,[a,b] GWANGHYUN JUNG,[a,e] ALEXANDER M. ZÖLLNER,[f] MALTE TIBURCY,[g,h] JOHANNES RIEGLER,[a,b] ELENA MATSA,[a,b] PRAVEEN SHUKLA,[a,b] YAN ZHUGE,[a,b] TONY CHOUR,[a,b] VINCENT C. CHEN,[i] PAUL W. BURRIDGE,[a,b] IOANNIS KARAKIKES,[a,b] ELLEN KUHL,[a,c,f] DANIEL BERNSTEIN,[a,e] LARRY A. COUTURE,[i,j] JOSEPH D. GOLD,[a,b] WOLFRAM H. ZIMMERMANN,[g,h] JOSEPH C. WU[a,b,c,d]

[a]Stanford Cardiovascular Institute, [b]Institute for Stem Cell Biology and Regenerative Medicine, [c]Bio-X Program, [d]Department of Medicine, Division of Cardiovascular Medicine, [e]Department of Pediatrics, Division of Cardiology, and [f]Department of Mechanical Engineering, Stanford University, Stanford, California, USA; [g]Institute of Pharmacology and Toxicology, Heart Research Center, University Medical Center, Georg-August-University, Göttingen, Germany; [h]DZHK (German Center for Cardiovascular Research) Partner Site, Göttingen, Germany; [i]Center for Biomedicine and Genetics; [j]Center for Applied Technology Development, City of Hope, Duarte, California, USA

*Contributed equally

Correspondence to: Joseph C. Wu, M.D., Ph.D., 265 Campus Drive, Room G1120B, Stanford, California 94305-5454, USA. Telephone: 650-736-2246; e-mail: joewu@stanford.edu; or Oscar J. Abilez, M.D., Ph.D., 265 Campus Drive, Room G1120B, Stanford, California 94305-5454, USA. e-mail: ojabilez@stanford.edu

Received October 5, 2015; accepted for publication October 23, 2017; first published online in STEM CELLS *EXPRESS* October 31, 2017.

http://dx.doi.org/10.1002/stem.2732

Key Words. Computational modeling • Cardiac • Tissue regeneration • Pluripotent stem cells • Calcium handling • Engineered heart muscle • Tissue engineering • Bioengineering • Cardiomyocyte • Heart

ABSTRACT

The ability to differentiate human pluripotent stem cells (hPSCs) into cardiomyocytes (CMs) makes them an attractive source for repairing injured myocardium, disease modeling, and drug testing. Although current differentiation protocols yield hPSC-CMs to >90% efficiency, hPSC-CMs exhibit immature characteristics. With the goal of overcoming this limitation, we tested the effects of varying passive stretch on engineered heart muscle (EHM) structural and functional maturation, guided by computational modeling. Human embryonic stem cells (hESCs, H7 line) or human induced pluripotent stem cells (IMR-90 line) were differentiated to hPSC-derived cardiomyocytes (hPSC-CMs) in vitro using a small molecule based protocol. hPSC-CMs were characterized by troponin$^+$ flow cytometry as well as electrophysiological measurements. Afterwards, 1.2 × 10^6 hPSC-CMs were mixed with 0.4 × 10^6 human fibroblasts (IMR-90 line) (3:1 ratio) and type-I collagen. The blend was cast into custom-made 12-mm long polydimethylsiloxane reservoirs to vary nominal passive stretch of EHMs to 5, 7, or 9 mm. EHM characteristics were monitored for up to 50 days, with EHMs having a passive stretch of 7 mm giving the most consistent formation. Based on our initial macroscopic observations of EHM formation, we created a computational model that predicts the stress distribution throughout EHMs, which is a function of cellular composition, cellular ratio, and geometry. Based on this predictive modeling, we show cell alignment by immunohistochemistry and coordinated calcium waves by calcium imaging. Furthermore, coordinated calcium waves and mechanical contractions were apparent throughout entire EHMs. The stiffness and active forces of hPSC-derived EHMs are comparable with rat neonatal cardiomyocyte-derived EHMs. Three-dimensional EHMs display increased expression of mature cardiomyocyte genes including sarcomeric protein troponin-T, calcium and potassium ion channels, β-adrenergic receptors, and t-tubule protein caveolin-3. Passive stretch affects the structural and functional maturation of EHMs. Based on our predictive computational modeling, we show how to optimize cell alignment and calcium dynamics within EHMs. These findings provide a basis for the rational design of EHMs, which enables future scale-up productions for clinical use in cardiovascular tissue engineering. STEM CELLS *2018;36:265–277*

SIGNIFICANCE STATEMENT

The ability to differentiate human pluripotent stem cells (hPSCs) into cardiomyocytes (CMs) makes them an attractive source for repairing injured myocardium, disease modeling, and drug testing. Although current differentiation protocols yield hPSC-CMs to greater than 90%, hPSC-CMs exhibit immature characteristics. With the goal of overcoming this limitation, the effects of varying passive stretch on engineered heart muscle (EHM) structure and function were tested. Guided by experimental observations and predictive computational modeling, it was shown how EHM maturation can be tuned. These findings are believed to be significant because the results provides a basis for the rationale design and scale-up of EHMs.

Introduction

Cardiovascular disease is the number one cause of morbidity and mortality in the Western world [1]. Following a myocardial infarction, cardiac tissue, comprising mainly cardiomyocytes (CMs), fibroblast cells (FCs), endothelial cells (ECs), and smooth muscle cells (SMCs), dies and there is little or no myocardial regeneration [2]. Instead, the dead myocardium is replaced with scar tissue, which often times leads to heart failure [3]. Thus, the delivery of replacement CMs by cardiomyoplasty or tissue engineering methods has emerged as a potential therapy because these approaches could restore function to an injured heart [2, 4, 5].

The proven ability to differentiate human pluripotent stem cells (hPSCs), which include both human embryonic stem cells (hESCs) [6] and human induced pluripotent stem cells (hiPSCs) [7], into CMs [8–11] make them an attractive source for repairing injured myocardium [2, 12–17], disease modeling [18–25], and drug testing [26–29]. Although the use of various biochemical differentiation protocols has increased current yields of hPSC-CMs to over 90% [9–11], hPSC-CMs do not typically exhibit adult phenotypes. Rather, they exhibit immature molecular, structural, and functional characteristics [30, 31].

In an effort to spatially and temporally organize hPSC-CMs toward a mature phenotype, methods and technologies that provide geometric [32], biochemical [33], electrical [34], optogenetic [35], and mechanical stimulation [14] in vitro mimicking the in vivo environment have been used to control function and improve maturity. These methods can upregulate cardiac-specific genes, activate stretch and voltage-gated ion channels, and drive enhanced formation of sarcomeric structures [30]. Additionally, hPSC-CMs have been used alone or in combination with FCs, ECs, SMCs, and mesenchymal stem cells, along with different extracellular matrices, and various forms of stimulation to tissue-engineer structures that enhance hPSC-CM organization and maturity [12, 14, 17, 24, 36–44].

Similarly, with the goal of enhancing hPSC-CM organization, here, we show the effect of passive stretch and the resulting stress on engineered heart muscle (EHM) gene expression, structural formation, calcium handling, and force generation. For a given material, normalized passive stretch and stress are related by the elastic modulus, or Young's modulus, of the material. The elastic modulus is a measure of inherent material stiffness, and for cardiac tissue, it ranges from 25–200 kPa, depending on the presence or absence of cardiac pathology [45, 46]. Furthermore, the elastic modulus in cardiac tissue depends on the composition and interplay of the extracellular matrix (ECM) (e.g., collagen and elastin), the various cellular components (e.g., CM, FC, EC, and SMC), and intracellular components (e.g., titin, microtubules, and intermediate filaments) [45, 47–49].

In our study, we describe how EHMs consisting of hPSC-derived cardiomyocytes (hPSC-CMs) mixed in a defined ratio with FCs (specifically the human fibroblast IMR-90 line) form over time, given fixed total starting cell numbers but grown at different passive lengths. We then use our macroscopic observations of EHM formation to create a computational model that predicts the stress distribution throughout EHMs. Based on this predictive modeling, we create EHMs with upregulated expression of genes associated with maturation, with aligned cardiomyocytes, and with coordinated calcium waves and mechanical contractions throughout.

Materials and Methods

Supporting Information Methods are available in the online-only Supporting Information Materials.

Negative Mold Design and Fabrication

A negative mold was designed using SolidWorks (Dassault Systèmes, Providence, RI) software and 3D-printed at the Stanford 3-Dimensional Printing Facility (Supporting Information Fig. S1). The inner diameter of the mold is 35.5 mm. Five rectangular reservoirs (3 mm $\times$ 12 mm $\times$ 3 mm) with curved edges are in the center and serve as the negative mold for reservoirs that hold the cell-ECM mixture. Each rectangle has two holes, which serve as the negative mold for post formation. The distance between the posts (center-to-center) is 5, 7, and 9 mm.

PDMS Mold Fabrication and Preparation

Polydimethylsiloxane (PDMS) was used to cast the molds for EHM formation (Supporting Information Fig. S1). PDMS was fabricated using the Sylgard Silicone Elastomer Kit (Dow Corning, Auburn MI, Fisher Scientific NC0162601). An 8:1 (w/v) ratio of 8 g of silicone base to 1 ml of activator was mixed, degassed in a vacuum chamber for 15 minutes, and poured into the negative molds. After a second degassing for 15 minutes, the cast PDMS molds were cured at 60F for at least 2 hours. The PDMS molds were cleaned in a sonicated water bath for 10 minutes and repeated with a clean water bath. Subsequently, the PDMS devices were sterilized in an autoclave for 35 minutes (20 minutes sterilization and 15 minutes drying).

hPSC Maintenance

hPSC consisting of hESC (H7 line, WiCell, Madison, WI) [6] and hiPSC (derived from IMR-90 line, Madison, WI) [50] were maintained in six-well tissue culture plates through daily feeding (2 ml per well) with E8 media (Life Technologies, Carlsbad, CA) as described previously [11] and detailed in the Supporting Information Methods.

hPSC-CM Differentiation

Our differentiation medium ("Complete RPMI") consisted of RPMI-1640 media (Life Technologies, Carlsbad, CA, 11875-085) supplemented with B27 minus insulin (Life Technologies, Carlsbad, CA, A1895601) (RPMI + B27-). To this medium, two small molecules were added over a week-long timetable as described previously [9, 11] and detailed in the Supporting Information Methods and shown in Supporting Information Figure S2.

hPSC-CM Electrophysiology

Whole cell action potentials (APs) were recorded with the use of standard patch-clamp technique, as described previously [11, 51] and detailed in the Supporting Information Methods. Criteria used for classifying observed APs into ventricular-, atrial-, and nodal-like hPSC-CMs are detailed in Supporting Information Figure S3A.

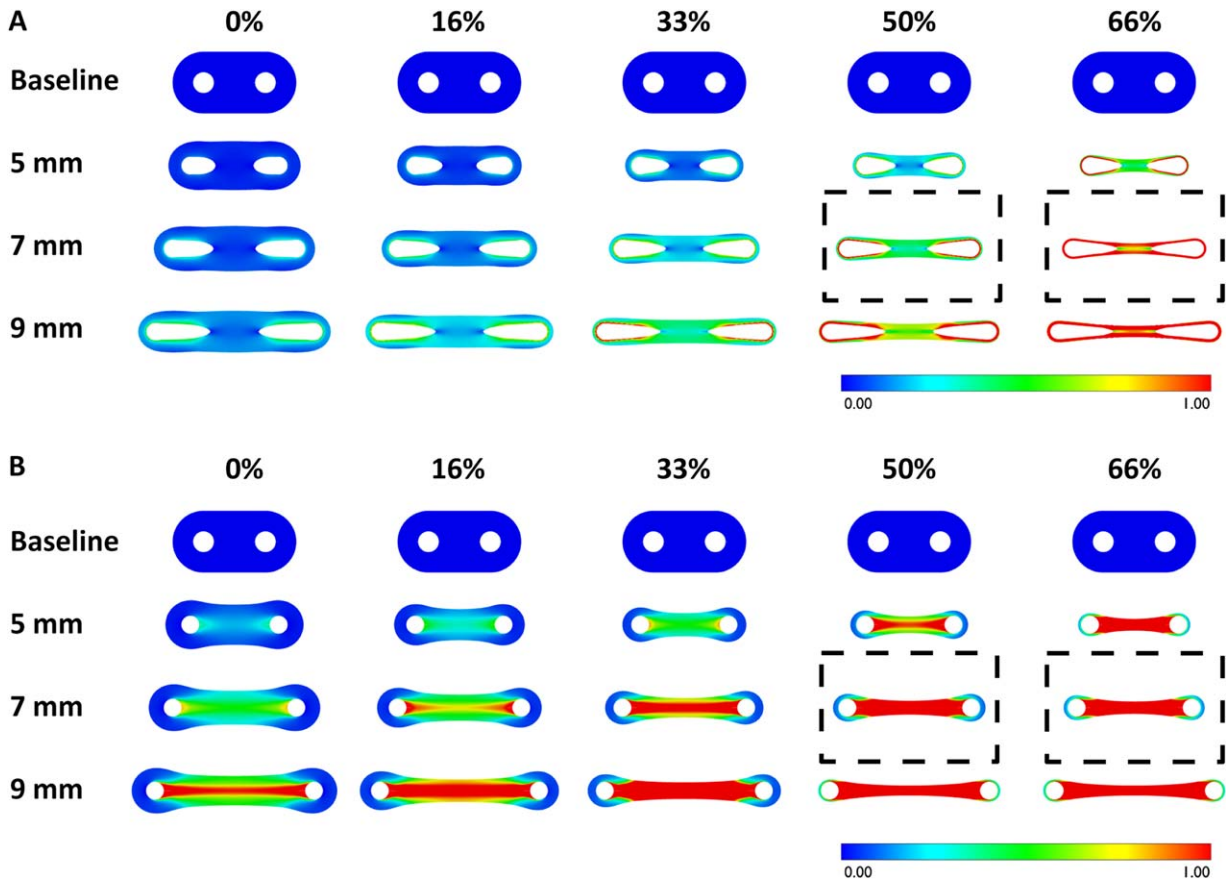

Figure 1. Computational modeling reveals spatial distribution of maximum principal stress in engineered heart muscle (EHM) for varying passive stretch and EHM compaction. **(A):** EHMs show low stresses in the center and the unpopulated areas next to the post holes, with the initial assumption that EHMs detach from the inner surface of the end posts during formation. V-necking is apparent at the site of the posts. **(B):** EHMs show higher stress in the center and increased thinning for increased EHM passive stretch, with the initial assumption that EHMs stay attached to the inner surface of the end posts during formation. Percentages along the top are volume compaction; baseline (no stretch), 5, 7, and 9 mm are the distances between the posts. Dashed rectangles highlight optimal geometries seen in experiments. Color code from 0.00 to 1.00 shows normalized stresses compared with baseline.

hPSC-CM Flow Cytometry

Flow cytometry was performed as described previously [11] and detailed in the Supporting Information Methods.

EHM Computational Modeling

A finite element model of the initial baseline non-compacted EHM was created using 345 linear 2D quadrilateral elements with 782 degrees of freedom using Abaqus (Dassault Systèmes, Providence, RI) (Fig. 1). The original shape of the low density cell-hydrogel-media mix was approximated by a rounded 3 mm $\times$ 6 mm rectangle with two PDMS posts separated by a baseline distance of 3 mm. To model different post distances, the EHM was stretched from its original post distance of 3 to 5 mm, 7 mm, and 9 mm, respectively. The subsequent compaction of the EHM was modeled by a gradual volume reduction following initial experimental observations. Parametric studies were performed by isotropically shrinking the EHM volume by 16.7%, 33.3%, 50.0%, and 66.7% compared with the 100% baseline volume. Additional parametric studies were performed to characterize the influence of EHM detachment. Because V-neck formation was observed experimentally, where EHMs detached from the inner surfaces of the posts as they compacted as shown in Figure 3A, the post-cell interface was detached by 0% and 100% at the inner hemi-circle surfaces of the posts.

EHM Generation and Formation

EHMs were generated by pre-mixing stem cell-derived cardiomyocytes, fibroblasts, and a collagen-based hydrogel as described previously [20, 36, 38, 42, 52, 53] and detailed in the Supporting Information Methods and shown in Figure 2A, 2B. Characteristics of EHM formation were observed daily for wall detachment, post detachment, opacity, and V-neck formation as shown in Figure 3A.

EHM Immunohistochemistry

Immunohistochemistry (IHC) was performed as described previously [11] and detailed in the Supporting Information Methods. Primary and secondary antibodies are listed in Supporting Information Table 1.

EHM Calcium Imaging

The Fluo-4 Direct Calcium Assay kit was used (Invitrogen, Carlsbad, CA, F10471) per manufacturer's instructions as described previously [22, 23] and detailed in the Supporting Information Methods. A motion decoupler was not used;

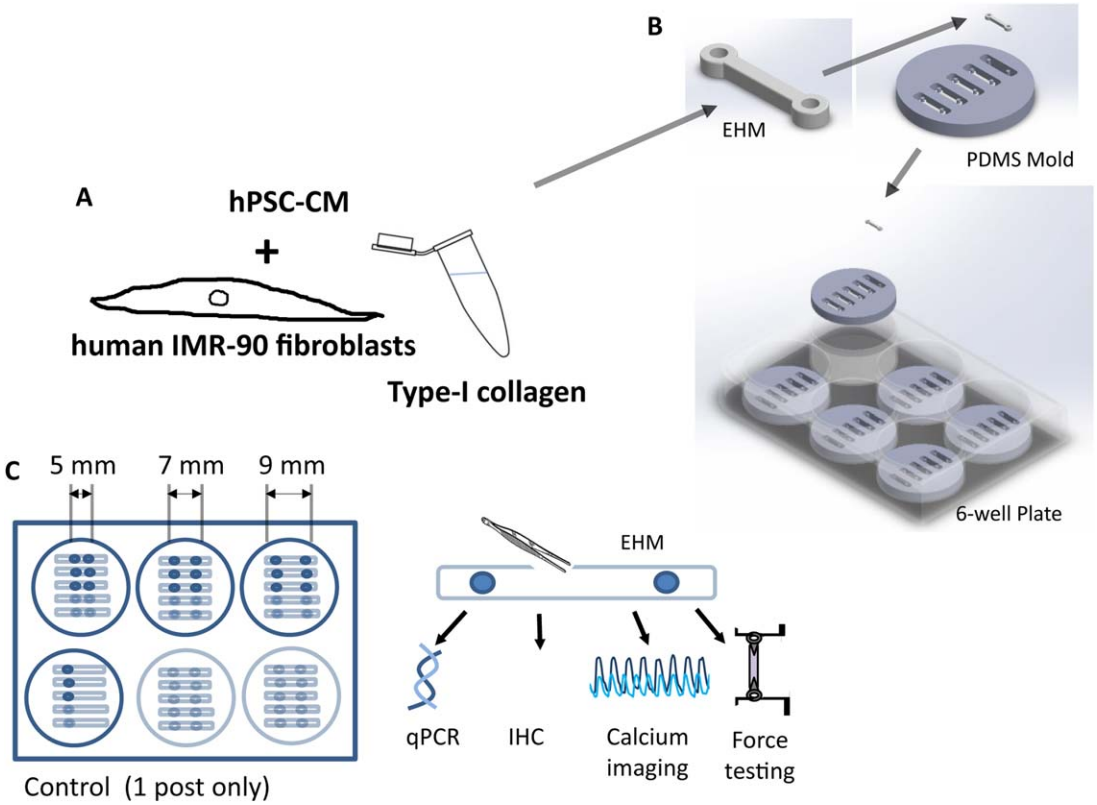

Figure 2. Generation and formation of engineered heart muscles (EHMs) of varying passive stretch. **(A):** Human pluripotent stem cell-derived cardiomyocytes and human fibroblasts (IMR-90 line) were mixed with type-I collagen to create EHMs. **(B):** The cell/collagen mixture was seeded into polydimethylsiloxane (PDMS) molds which contain five 100 μl reservoirs and fit within the wells of a six-well dish. **(C):** EHM were cast in reservoirs containing two PDMS posts spaced at 5, 7, and 9 mm or containing only one post (control with no tension). EHMs were allowed to condense and were analyzed at various time points within days 1–50 by quantitative polymerase chain reaction, immunohistochemistry, calcium imaging, and force testing. Abbreviations: CM, cardiomyocytes; EHM, engineered heart muscle; hPSC, human pluripotent stem cell; IHC, immunohistochemistry; PDMS, polydimethylsiloxane; qPCR, quantitative polymerase chain reaction.

however, regions of interest (ROI) were defined, and averaging was performed in each ROI. Calcium transients were analyzed with a custom analytical MATLAB (MathWorks, Natick, MA) script and validated as shown in Supporting Information Figure S4.

EHM Stress–Strain Relationship and Elastic Modulus

Each EHM was mounted to a force transducer using vascular clamps at either end of the EHM. The EHM was stretched 15 μm in 15 second intervals. In response to stretch, the EHM displays an immediate increase in force (also known as systolic force, with a parallel increase in diastolic force) then relaxes until it reaches a new steady state. The time interval is long enough to allow for a new steady state to develop. The linear relationship between stress and strain is the Young's modulus. Maximum active force (also known as twitch force, which is the difference between systolic force and diastolic force) is calculated by the average of the 10 highest active forces.

EHM Gene Expression

Quantitative polymerase chain reaction (qPCR) was performed using primers for β1-adrenergic receptor (*ADRB1*), β2-adrenergic receptor (*ADRB2*), caveolin-3 (*CAV3*), potassium ion channel (*KCNJ2*), troponin-T (*TNNT2*), and calcium ion channel (*CACNA1C*). Total RNA was isolated from hPSC-CMs cultured in monolayer or as EHMs according to the manufacturer's protocol (RNeasy Mini Kit; Qiagen, Valencia, CA). Primers for *TNNT2* were obtained from TaqMan (Applied Biosystems, Foster City, CA) assay (Hs 00165960) and other primers were designed using PrimerBank (http://pga.mgh.harvard.edu/primerbank/) shown in Supporting Information Table 2. A 50-ng total RNA were reverse transcribed to cDNA and amplified over 40 cycles using the CFX384 Bio-Rad thermocycler (Bio-Rad Laboratories, Hercules, CA). One-step qPCR using SYBR green technology (Qiagen, Hilden, Germany) was performed. Expression of cardiac genes was confirmed for each condition and normalized to the housekeeping genes GAPDH using the 2 power ($-\Delta\Delta$Ct) method.

Statistical Analysis

Unless otherwise specified, an unpaired two-tailed Student's *t* test was used to calculate significant differences between two groups and data are expressed as mean ± SD. For calcium dynamics and qPCR, statistical analyses were performed using JMP Pro 13.1 (SAS Institute Inc, Cary, NC) and GraphPad Prism (GraphPad Software, La Jolla, CA). Data are expressed as mean ± SEM. For calcium dynamics, differences between groups were assessed by using both Student's *t* test and one-way analysis of variance followed by Tukey's post hoc testing. A $p < .05$ was considered statistically significant for calcium dynamics and qPCR.

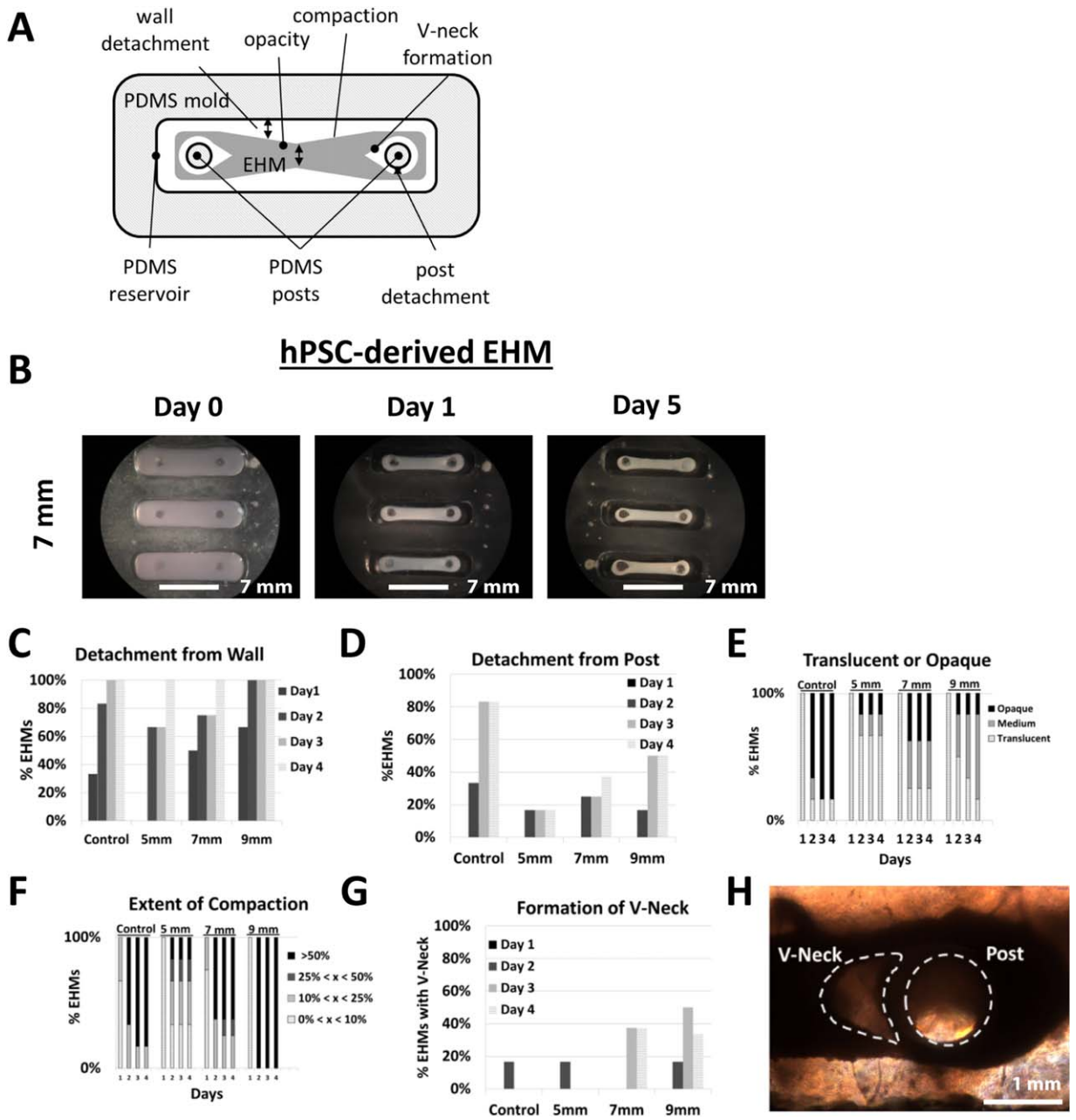

Figure 3. Engineered heart muscle (EHM) formation depends on passive stretch. **(A):** EHMs were observed daily for wall detachment, post detachment, opacity, compaction, and V-neck formation. **(B):** Human pluripotent stem cell-derived cardiomyocytes were mixed with fibroblasts (IMR-90 line) and type-I collagen and seeded into custom-designed PDMS molds. EHM formation was monitored over time (days 0–5). Inter-post distance of a representative EHM is 7 mm. A single post (conferring no tension) served as a control. White scale bar = 7 mm. Daily observations of EHM formation according to predetermined criteria by percentage EHMs, including **(C)** detachment from the reservoir walls, **(D)** detachment from posts, **(E)** opacity, **(F)** extent of compaction, and **(G, H)** formation of a tension-induced V-neck at EHM-anchoring end posts. White scale bar = 1 mm (H). Abbreviations: EHM, engineered heart muscle; hPSC, human pluripotent stem cell; PDMS, polydimethylsiloxane.

Results

hPSC-CM Electrophysiology

hPSC-CMs at days 25–28 demonstrated a heterogeneous phenotype, with ventricular-like cells being the predominant phenotype (57%) along with atrial-like (24%) and nodal-like (19%) cells (Supporting Information Fig. S3B, S3C). Patch-clamp analysis demonstrated that the average maximum diastolic potential of ventricular-like (V-like) cells were -63.3 ± 1.7 ($\pm$SEM), and the maximal upstroke velocity (V_{max}) measured as V/s was 27.4 ± 1.8 (Supporting Information Fig. S3D).

hPSC-CM Flow Cytometry

Before EHMs were formed, hPSC-CMs were characterized using flow cytometry for sarcomeric protein troponin-T. A representative differentiation of hiPSC-CM yielded 88% troponin-T–positive cells (Supporting Information Fig. S5). City of Hope manufacturing records revealed that the lot of hESC-CMs (70

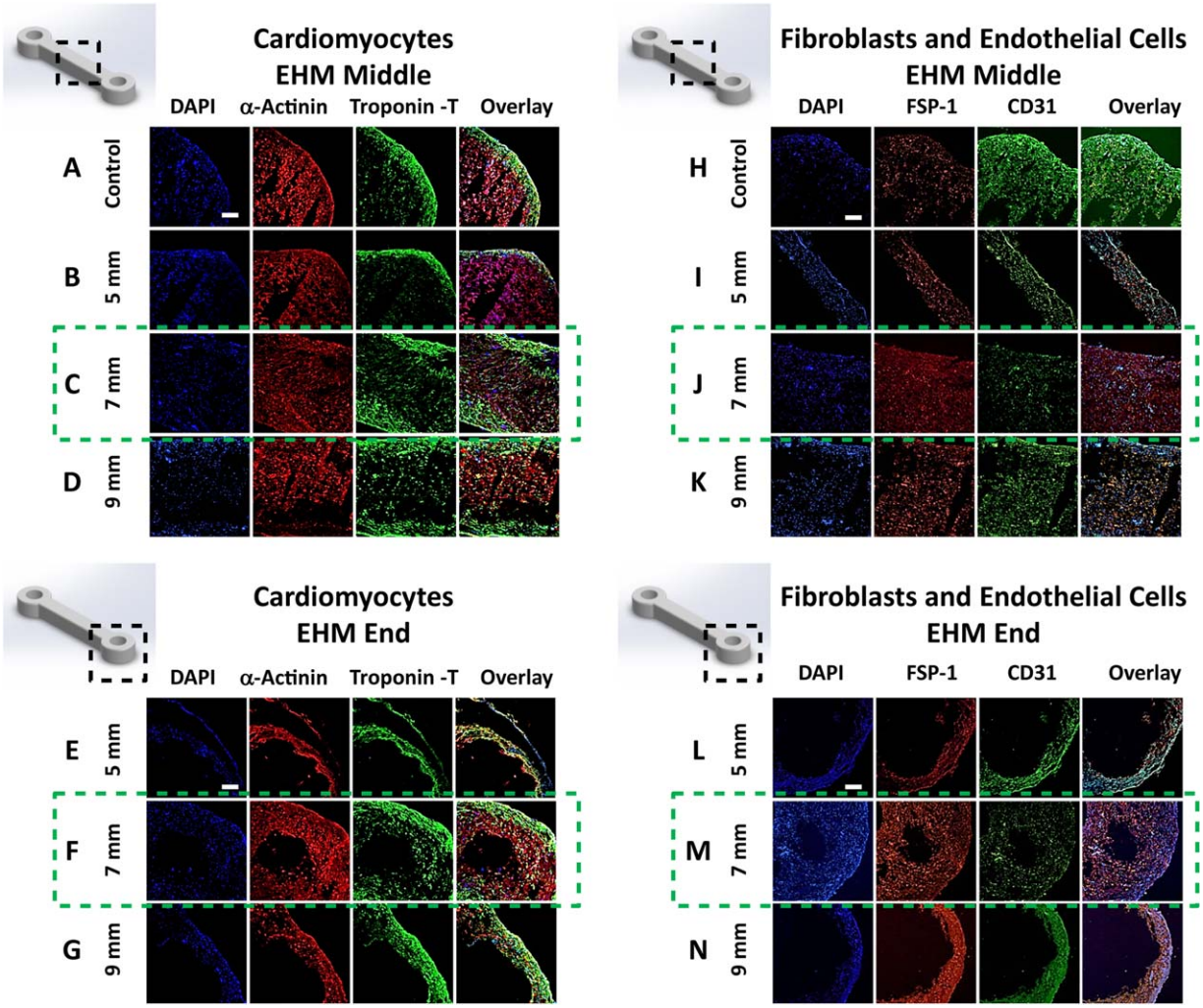

Figure 4. Low magnification immunohistochemistry shows cardiovascular cell types are present in engineered heart muscles (EHMs) and distribution depends on passive stretch. **(A–D):** At the EHM middle, cardiomyocytes labeled with α-actinin (red) and troponin-T (green) are present throughout the EHM width, with Troponin-T expressed most highly at the EHM outer edges. **(E–G):** At the EHM ends, cardiomyocytes labeled with α-actinin (red) and troponin-T (green) are also present throughout the EHM width, with troponin-T expressed most highly at the EHM outer edges. **(H–K):** At the EHM middle, fibroblasts labeled with FSP-1 (red) and endothelial cells labeled with CD31 (green) are homogeneously present throughout the EHM width. **(L–N):** At the EHM ends, fibroblasts labeled with FSP-1 (red) and endothelial cells labeled with CD31 (green) are also homogeneously present throughout the EHM width. (C, F, J, M) The 7 mm passive stretch shows the most organized morphology (dashed green rectangles). In all panels, 4′,6-diamidino-2-phenylindole labels cellular nuclei. White scale bar = 100 μm (A, E, L, N). Objective magnification is ×10. Abbreviations: DAPI, 4′,6-diamidino-2-phenylindole; EHM, engineered heart muscle; FSP-1, fibroblast specific protein-1.

million CMs per lot) used to fabricate EHMs were 71% troponin-T positive. These results are consistent with our previously published differentiation yields [11].

EHM Computational Modeling

The normalized maximum principal stress of EHMs under passive stretch was analyzed for different parameter combinations. Figure 1 illustrates the different shapes and stress distributions for varying post distances (and varying passive stretch), compaction levels, and detachment of the EHM from the posts. For 100% detachment (Fig. 1A) and 0% detachment (Fig. 1B) from posts at both ends, we observe the characteristic scenarios with and without V-neck formation. With 100% detachment (Fig. 1A), there are elongated, unpopulated areas between the posts and EHM, areas of low stress in the center, and moderate V-necking (<15%) for up to 33% EHM compaction upon EHM formation. With 50% or more compaction, V-necking increases significantly (>25%). V-necking and maximum principal stresses (shown maximally in red) increase with EHM compaction during EHM formation. With 0% detachment from the posts (Fig. 1B), high principal stresses (shown maximally in red) exist in the EHM center and no unpopulated areas are evident next to the posts. Stresses are significantly higher (35%–55%) across all compaction levels compared with the 100% detachment scenario. Again, maximum principal stresses increase with EHM compaction upon EHM formation. Our subsequent experiments below revealed that EHMs showed low stresses within central internal areas and the unpopulated areas next to the post holes (Figs. 3–5), thus supporting our initial assumption that EHMs detach from the inner surface of the end posts during formation (Fig. 1A). Furthermore, our subsequent experiments showed calcium dynamics correlates with EHM passive stretch (Fig. 6)

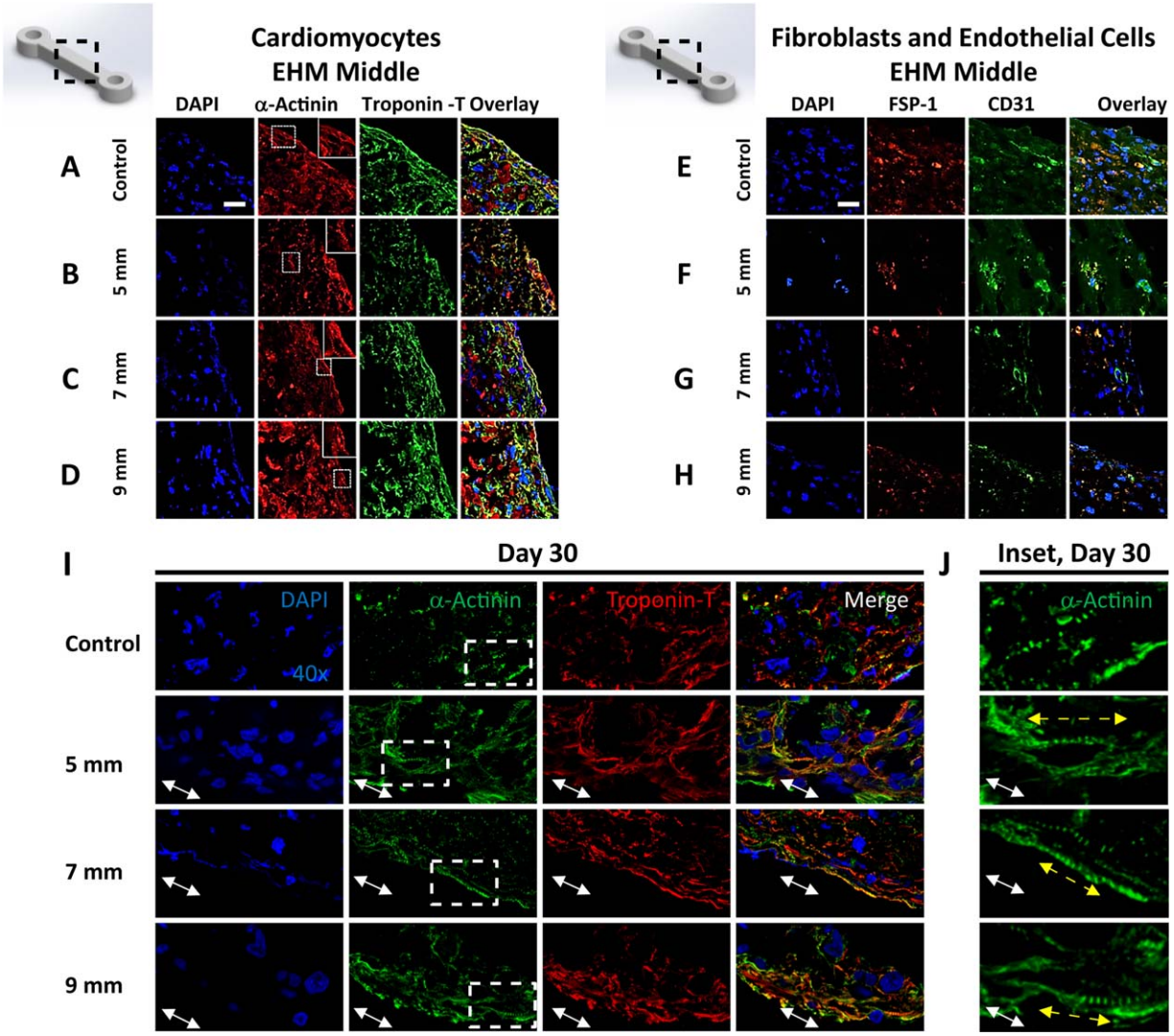

Figure 5. High-magnification immunohistochemistry shows cardiovascular cell types are present in engineered heart muscles (EHMs) with various sarcomeric organization at different passive lengths. **(A–D):** At the EHM middle and outer edges, cardiomyocytes labeled with α-actinin (red) and troponin-T (green) are present, with sarcomeric banding patterns visible at all lengths as shown in insets. **(E–H):** At the EHM middle and outer edges, fibroblasts labeled with FSP-1 (red) and endothelial cells labeled with CD31 (green) are present. **(I):** Representative images of day 30 EHMs show various degrees of cardiomyocyte sarcomeric alignment at control, 5, 7, and 9 mm passive stretch as demonstrated by α-actinin (green) and troponin-T (red) immunostaining. White double-ended arrows indicate the primary direction of stretch. **(J):** High-magnification views of the area insets indicated by the white dashed rectangles in (I). White double-ended arrows indicate the primary direction of stretch while yellow double-ended dashed arrows indicate the general direction of sarcomeric alignment. EHMs under 7 mm stretch demonstrated sarcomeres most aligned with the primary direction of stretch as compared with control, 5, and 9 mm groups. In all panels, 4′,6-diamidino-2-phenylindole labels cellular nuclei. White scale bar = 20 μm (A, E). Objective magnification is ×63 in (A–H) and ×40 in (I). Abbreviations: DAPI, 4′,6-diamidino-2-phenylindole; EHM, engineered heart muscle; FSP-1, fibroblast specific protein-1.

EHM Generation

PDMS molds contained five reservoirs, each holding 100 μl of a mixture of hPSC-CMs consisting of either hESC-CMs (H7 line) or hiPSC-CMs (IMR-90 line), human fibroblasts (IMR-90 line), and type I-collagen (Fig. 2A, 2B). Before EHMs were formed hPSC-CMs were characterized using flow cytometry for sarcomeric protein troponin-T. A representative differentiation of hiPSC-CM yielded 88% troponin-T–positive cells (Supporting Information Fig. S5). City of Hope manufacturing records revealed the lot of hESC-CMs (70 million CMs per lot) used to fabricate EHMs were 71% troponin-T positive. These results are consistent with our previously published differentiation yields [11]. hPSC-CMs and fibroblasts (IMR-90 line) were mixed in a 3:1 ratio. This ratio was confirmed to yield better compaction of EHMs than without fibroblasts (Supporting Information Fig. S6). Posts in the reservoir were spaced at 5 mm, 7 mm, or 9 mm apart (Fig. 2; Supporting Information Fig. S1). The no-tension control was based on the 9 mm configuration with one post physically removed.

EHM Formation

Formation of EHMs was assessed as a series of observational measures beginning with detachment from the reservoir's wall, detachment from the posts, opacity, extent of compaction, and formation of tension-induced V-neck (Fig. 3A, 3C–

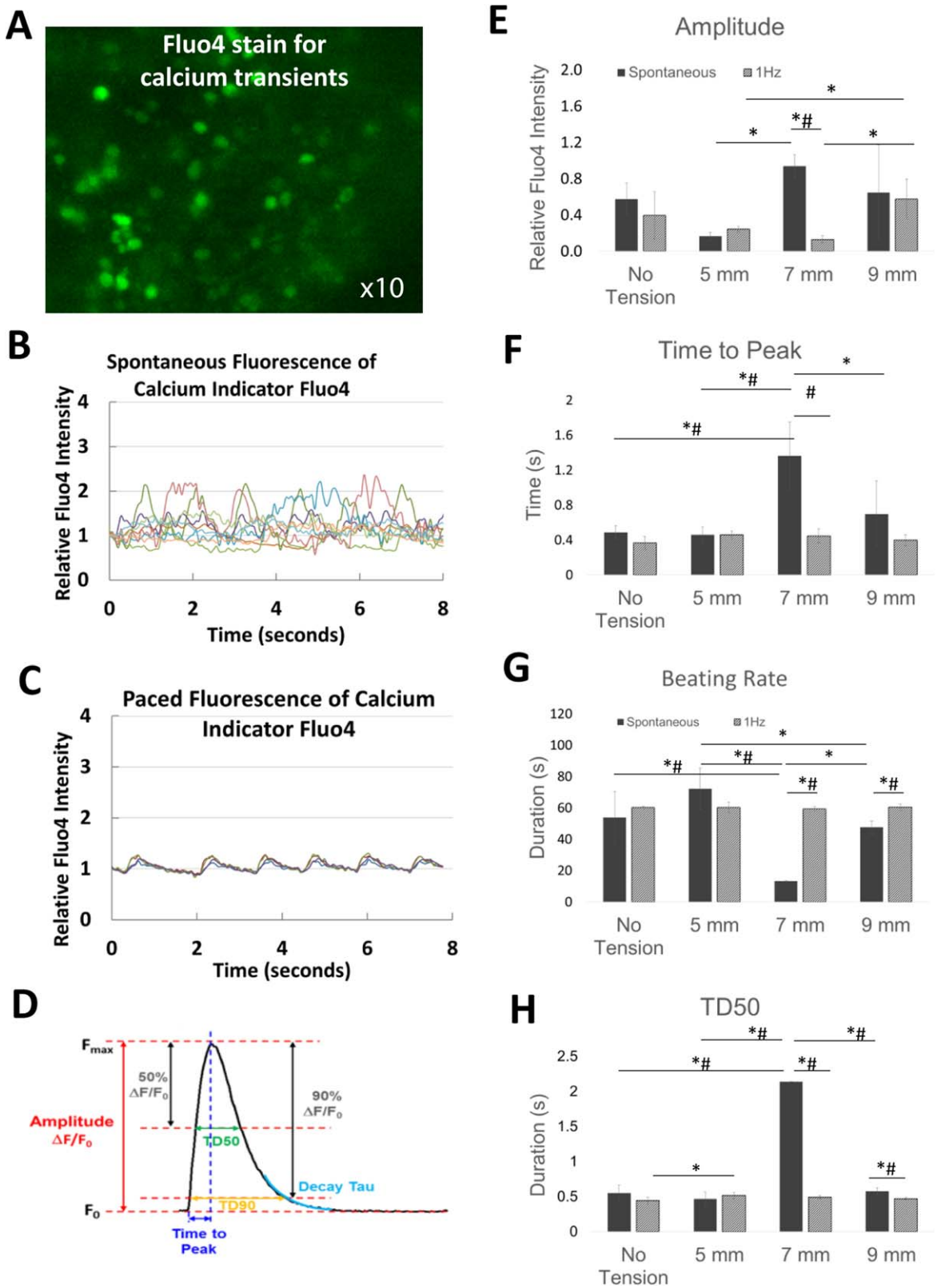

Figure 6. Calcium dynamics correlates with engineered heart muscle (EHM) passive stretch. **(A):** Representative image of Fluo-4 staining to detect calcium transients. Objective magnification is ×10. **(B, C):** Relative Fluo-4 intensities over time with and without electrical stimulation at 1 Hz. **(D):** Calcium imaging waveform analytical parameters. Analytical outputs for spontaneous and electrically paced EHMs at 5, 7, and 9 mm interpost distances: **(E)** amplitude, **(F)** time-to-peak, **(G)** beating rate, and **(H)** TD50. Each colored waveform in (B) is a representative waveform of the spontaneous, non-paced calcium dynamics of EHMs ($n = 12$) generated under tension at 7 mm stretch. The mean beating rates of all stretch conditions for both spontaneous and paced groups are shown in (G). Mean ± SEM. *, $p < .05$ (Student's t test); #, $p < .05$ (one-way analysis of variance with Tukey's post hoc testing).

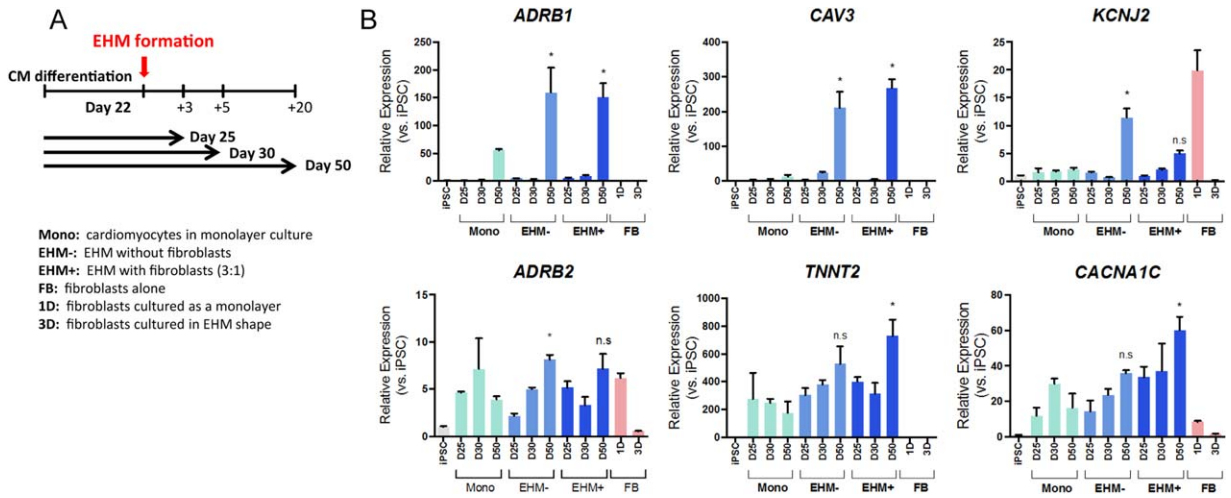

Figure 7. Engineered heart muscle (EHM) gene expression indicates increased maturation of cardiomyocytes. **(A):** EHMs (7 mm inter-post distance) were formed with day 22 cardiomyocytes and were matured until days 25, 30, and 50. **(B):** Quantitative polymerase chain reaction analysis was performed using primers for β1-adrenergic receptor (*ADRB1*), calveolin-3 (*CAV3*), potassium ion channel (*KCNJ2*), β2-adrenergic receptor (*ADRB2*), troponin-T (*TNNT2*), and calcium ion channel (*CACNA1C*). Gene expression in EHM+ samples were normalized by the ratio of cardiomyocytes to fibroblast (3:1). Compared with day 50 cardiomyocytes, day 50 expression of *ADRB1*, *CAV3*, *TNNT2*, and *CACNA1C* of EHMs with fibroblasts (EHM+) was all statistically significantly increased. Mean ± SEM. *, $p < .05$ versus day 50 monolayer cardiomyocytes (one-way analysis of variance with Tukey's post hoc testing). Abbreviations: CM, cardiomyocytes; EHM, engineered heart muscle; iPSC, induced pluripotent stem cell.

3H). V-neck is the space that appears between the post inner surface and the EHM as the EHM under tension pulls away from the post. Formation of EHMs was observed up to day 9 with condensation typically plateauing at day 5 (Fig. 3B); the sample size was $n = 5$, 3, 4, and 3 for control-, 5 mm-, 7 mm-, and 9 mm-EHMs, respectively (Fig. 3C–3H).

Although all EHMs detached from the reservoir's wall (Fig. 3C), the 9 mm-EHMs displayed fastest detachment by day 2. The greatest detachment from posts was evident in the controls (which were designed to have 1 post) and the 9 mm-EHMs (Fig. 3D). Opacity is a consequence of compaction, and thus, the greatest opacity occurred in the control where EHMs formed as a clump around one post (Fig. 3E). The 9 mm-EHMs also showed fastest compaction such that all 9 mm-EHMs compacted 50% or more by day 2 compared with 5 mm, 7 mm, and no tension controls (Fig. 3F). The percent of EHMs formed with 9 mm posts showed greatest V-neck formation at day 3, which subsequently decreased at day 4 due to breakage or detachment from posts (Fig. 3G). An example of V-neck formation is shown in Figure 3H. Despite having the best compaction (Fig. 3F) and tension (Fig. 3G), the 9 mm post distance also displayed the greatest rate of detachment from the posts (Fig. 3D). Most no-tension controls naturally compacted around the single post; however, some of the controls attached to a topographical artifact of the severed post. For Figure 3C–3G, the sample size was $n = 6$, 6, 8, and 6 for control-, 5 mm-, 7 mm-, and 9 mm-EHMs, respectively.

EHM Immunohistochemistry

Low-magnification IHC shows cardiovascular cell types present in EHMs and their distribution depends on passive stretch (Fig. 4). At the EHM middle, cardiomyocytes labeled with α-actinin (red) and troponin-T (green) were present throughout the EHM width, with troponin-T expressed most highly at the EHM outer edges (Fig. 4A–4D). At the EHM ends, cardiomyocytes labeled with α-actinin (red) and troponin-T (green) were also present throughout the EHM width, with troponin-T expressed most highly at the EHM outer edges (Fig. 4E–4G). At the EHM middle, fibroblasts labeled with FSP-1 (red) and endothelial cells labeled with CD31 (green) were homogeneously present throughout the EHM width (Fig. 4H–4K). This indicated that the IMR-90 fibroblasts mixed in a 1:3 ratio with cardiomyocytes in the initial generation of EHMs, along with any fibroblasts already present in the cardiomyocyte differentiation cultures, survive within the EHMs. Furthermore, the observation that fibroblasts are also present throughout the EHM interior indicates adequate oxygenation is present throughout the EHMs. The presence of endothelial cells was likely from the initial cardiomyocyte differentiation cultures and the presence of cardiovascular progenitors, as has been reported by others [54], as we did not add exogenous endothelial cells in the generation of the EHMs. We validated the antibodies for FSP-1 and CD31 against human lung fibroblasts and human umbilical vein endothelial cells (HUVEC) as shown in Supporting Information Figure S7A. At the EHM ends, fibroblasts labeled with FSP-1 (red) and endothelial cells labeled with CD31 (green) were also homogeneously present throughout the EHM width (Fig. 4L–4N). The 7-mm passive stretch showed the most organized morphology (Fig. 4C, 4F, 4J, 4M, dashed green rectangles). To further confirm endothelial identity, we stained control EHMs with VE-Cadherin as shown in Supporting Information Figure S7B, S7C, which showed structures with branching morphology.

High-magnification IHC shows cardiovascular cell types were present in EHMs with sarcomeric organization at all passive lengths (Fig. 5). At the EHM middle and outer edges, cardiomyocytes labeled with α-actinin (red) and troponin-T (green) were present, with sarcomeric banding patterns visible at all lengths as shown in the insets in Figure 5A–5D. At the EHM middle and outer edges, fibroblasts labeled with FSP-1 (red) and endothelial cells labeled with CD31 (green) were present (Fig. 5E–5H). In Figure 5I, representative images of day 30

EHMs show various degrees of cardiomyocyte sarcomeric alignment at control, 5, 7, and 9 mm passive stretch as demonstrated by α-actinin (green) and troponin-T (red) immunostaining. White double-ended arrows in the figure indicate the primary direction of stretch. Figure 5J shows high-magnification views of the area insets indicated by the white dashed rectangles in Figure 5I. White double-ended arrows in the figure indicate the primary direction of stretch while yellow double-ended dashed arrows indicate the general direction of sarcomeric alignment. EHMs under 7 mm stretch demonstrated sarcomeres most aligned with the primary direction of stretch as compared to control, 5, and 9 mm groups.

To visualize the early time-course of sarcomeric organization and alignment, for samples at days 1, 5, and 9, EHM sections were immunostained with troponin-T to visualize cardiomyocytes and 4′,6-diamidino-2-phenylindole to visualize all nuclei (Supporting Information Fig. S8A–S8D). At day 5, 7 mm- and 9 mm-EHMs showed more alignment than 5 mm-EHMs and controls. Additionally, at day 9, alignment was apparent in the 5 mm-, 7 mm-, and 9 mm-EHMs. Supporting Information Figure S8E shows sarcomeres present at day 9 in 5 mm- and 7 mm-EHMs.

EHM Calcium Dynamics

Calcium transients were detected in EHMs at day 5 (Fig. 6A) after initial seeding, but not at day 1. At day 5, EHMs displayed spontaneous transients (Fig. 6B) as well as response to field stimulation at 1 Hz (Fig. 6C). Spontaneous and field-stimulated electrically evoked calcium transients can be seen propagating through an EHM at day 5 (Supporting Information Movies S1, S2). In addition, mechanical contractions were visibly detectable with the naked eye (Supporting Information Movie S3). Calcium transients were analyzed for amplitude, time-to-peak, beating rate, and TD50 (Fig. 6D). In samples under moderate tension (7 mm-EHMs), spontaneous contractions trended toward greater amplitudes (Fig. 6E), but were not statistically significantly different. However, the times-to-peak were longer (Fig. 6F) (*#, $p < .05$), and beating rates were slower (Fig. 6G) (*#, $p < .05$). As seen in Figure 6H, the parameter related to calcium recycling, TD50, was significantly greater for 7 mm-EHMs (*#, $p < .05$). When field stimulated at 1 Hz, the EHMs displayed calcium transients with similar waveform properties (Fig. 6E–[6]H).

EHM Stress–Strain Relationship and Elastic Modulus

The linear relationship of stress and strain reveals the elastic modulus or the Young's modulus. The measurement occurs in the linear phase before the plateau phase begins (Supporting Information Fig. S9A). EHMs were mounted onto a force transducer using vascular clamps (Supporting Information Fig. S9B) and were stretched 15 μm in 15 seconds intervals (Supporting Information Fig. S9C). In response to stretch, EHMs displayed an immediate increase in force (both a parallel increase in systolic and diastolic force) (Supporting Information Fig. S9D). EHMs proceeded to relax until reaching a new steady state. The time interval is long enough to allow for a new steady state to develop (Supporting Information Fig. S9E). The stiffness, as represented by Young's modulus, was comparable between EHMs fabricated from hPSC-derived CMs (66 kPa) or rat neonatal derived-CMs (160 kPa) (Supporting Information Fig. S9F) and the maximum active force (twitch force) was also comparable between human (0.5 mN) and rat (0.4 mN) EHMs (Supporting Information Fig. S9G). There was no statistical difference between the stiffness of the human and rat EHMs ($p < .35$) and no statistical difference between the maximum active force of the human and rat EHMs ($p < .11$).

EHM Elastic Behavior

EHMs under passive stretch remain highly elastic as is evident when passive stretch is removed. EHMs were allowed to form under passive stretch for 5 days ($n = 3$) (Supporting Information Fig. S10A). At this point, EHMs were released from their posts and observed for a subsequent 24 hours to day 6 (Supporting Information Fig. S10B). The length of the detached EHMs decreased to less than half of their original length (Supporting Information Fig. S10C–S10D). The detached length is similar to the length of control EHMs that formed on a single post without the influence of passive stretch. The relaxed EHM length is approximately 40% of the passive stretch length (Supporting Information Fig. S10C–S10D) at days 5 and 6. This amount of strain is about twice the physiological systolic strain of human heart muscle, which is about 12% to 22% upon volume loading [55]. However, the 24-hour post-mortem volume of a completely emptied heart (and, thus, in a fully relaxed state) has been estimated to range from 3% to 52%, with an average of 32%, of the in vivo diastolic volume [56, 57]. This compares more closely with the change seen between a stretched and relaxed EHM.

EHM Gene Expression

The effects of passive tension on the gene expression profile of mature cardiomyocyte genes were tested using our EHM platform. EHMs (7 mm inter-post distance) were formed using day 22 cardiomyocytes and matured until days 25, 30, and 50, which equates to 3 days, 8 days, and 28 days of maturation as a 3D structure (Fig. 7A). EHMs were formed with and without fibroblasts or with fibroblasts alone. As a 1D control, monolayers of cardiomyocytes were cultured for the same lengths of time. To control for gene expression in fibroblasts, 1D and 3D controls consisting of only fibroblasts were also included in the analysis. Both 3D structure and time increase the expression of genes related to the maturity of cardiomyocytes including β-adrenergic receptors 1 and 2 (*ADRB1* and *ADRB2*), calveolin-3 (*CAV3*), potassium (*KCNJ2*) and calcium ion channels (*CACNA1C*), and troponin-T (*TNNT2*) (Fig. 7B). *ADRB1* and *CAV3* have been shown as late onset markers in prolonged 1D culture (over day 60 in monolayer) and their expressions were enhanced by 2D culture [58]. In a 3D structure, *ADRB1* and *CAV3* expression was significantly increased 3-fold and over 15-fold versus 1D culture at day 50, respectively, suggesting that the EHM format shortens the time necessary to attain a more mature phenotype of hPSC-CMs. Similarly, potassium and calcium ion channels (*KCNJ2* and *CACNA1C*) and troponin-T (*TNNT2*) are highest in late-stage EHMs compared with 1D samples and early-stage EHMs. In contrast, *ADRB2* expression had similar levels in 1D and 3D structures at all time points. The age of the EHM, despite the absence or presence of fibroblasts, is important for the expression of all six genes and the maturation of EHMs. Day 50 EHMs display the highest levels of gene expression compared with days 30 or 25. Fibroblasts did not express, or had very low expression of, *ADRB1*, *CAV3*, *CACNA1C*, and *TNNT2*.

Compared with day 50 cardiomyocytes, day 50 expression of *ADRB1*, *CAV3*, *TNNT2*, and *CACNA1C* of EHMs with fibroblasts were all statistically significantly increased.

Discussion

The results presented here elucidate the effects of passive stretch on EHM formation and function through gene expression, cell alignment, calcium dynamics, and force generation within EHMs as predicted by computational modeling. Furthermore, analytic methods are described for calcium transient analysis and metrics to monitor EHM formation and compaction over time. Using experimental results, a computational model has been created that predicts the spatial distribution of maximum principal stress in EHMs for varying passive stretch and compaction levels. Time is an important factor in the development of internal forces and is represented as the percentage of volume compaction during the collagen-based hydrogel condensation. Initial passive tension, which is dictated by inner post distance, also affects the development of the force profile by increasing the speed by which the force profile develops. The difference in compaction between models A and B (Fig. 1) could be due to the interaction of the reservoir's surface with the hydrogel-cellular mixture during EHM formation. As the model demonstrates, this interaction is critical to the final distribution of forces and will affect the force profile of the EHM core versus outer layers as well as the thinnest regions around the posts. With these and future comprehensive experimental parameters, further refined computational models that are predictive of EHM structure and function can be created and can serve as a baseline for scaling EHMs toward clinical applications.

Modulating the resulting passive stress of EHMs may be important in accurately modeling pressure and volume overload cardiomyopathies. Either an increase or a decrease in passive cardiac stiffness can be detrimental [45]. For example, systolic pressure-overload, as in hypertrophic cardiomyopathy, results in a stiffer ventricle and impaired filling. In contrast, severe volume overload, as in dilated cardiomyopathy, results in a less stiff and more easily stretched ventricle and ultimately ventricular dilatation with functional consequences. Thus, EHMs provide a flexible platform for studying the consequences of overload in diseased tissue.

Three-dimensional structure and force conditioning improves the cardiac model by promoting cardiomyocyte maturation. As in the heart where contractile forces are enhanced by ventricular stretch upon filling [59], EHMs also respond to mechanical forces [14, 44, 59]. An increase in principal stress due to passive strain will increase alignment as demonstrated above and in other studies [14, 52, 60, 61]. In addition, 3D structure yields a faster and greater expression of genes present in mature cardiomyocytes. For example, troponin-T is a protein of the sarcomere and the contractile machinery of the cell [62]. Caveolin-3 induces the formation of caveolae and the T-tubule system, which facilitates membrane depolarization and the development of cellular contractions [58, 63, 64]. Ion channel proteins including sodium, calcium, and potassium facilitate excitation-contraction coupling, one of the fundamental properties of cardiomyocytes [65]. Finally, the upregulation of β-adrenergic receptors 1 and the relatively unchanged expression of β-adrenergic receptors 2 is also an indicator of maturation, and ensures responsiveness to β-adrenergic drug agonists and antagonists, which is important in testing this drug class [58]. As shown above, 3D EHM structure plays an important role in the genes that regulate AP generation and propagation.

The ability to create patient-specific hiPSCs has enabled the development of new disease models. Somatic cells can be obtained readily from patients with a variety of genetic diseases, reprogrammed to a pluripotent state, and differentiated to the cell type that recapitulates the disease phenotype [7, 50]. Subsequently, a variety of electrically and mechanically based cardiac diseases have indeed been modeled with hiPSCs [18, 19, 21–23]. The read-outs for these studies have typically been at the single cell level; however, for diseases that manifest at the tissue level, generation of EHMs that faithfully recapitulate the disease phenotype will be necessary [38, 66]. For example, monitoring EHM formation or malformation [45] may serve as a model for assessing congenital heart disease such as left ventricular non-compaction where malformation of cardiac structures leads to the dominant disease phenotype rather than being caused by defects in individual cardiomyocytes per se. In at least three of the above studies [21–23], calcium dynamics were abnormal, and thus the results presented here on the modulation of EHM calcium dynamics by varying passive stretch will be useful in future disease modeling studies.

Conclusion

In summary, this study focused on the rational design of EHMs based on the extent of passive stretch on gene expression, cell alignment, calcium dynamics, and force generation within EHMs. The findings will be important in creating EHMs that give insight into fetal, neonatal, pediatric, and adult human cardiac tissue physiology and pathophysiology, drug screening, and toxicity testing. Recent reports on the calcium dynamics of ex vivo human cardiac tissue slices [67] provide a benchmark for the calcium dynamics of these EHMs. Moreover, future strategies will likely incorporate biochemical [33], electrical [34], optogenetic [35], and active mechanical stimulation [14] with the goal of spatially and temporally organizing hPSC-CMs and directing them toward a more mature phenotype. Finally, the combination of computational modeling for EHM rational design as well as the evolving maturation strategies for EHM structure and function will enable the future scale-up of EHMs for clinical use.

Acknowledgments

We thank the Stanford 3-Dimensional Printing Facility, Stanford Institute for Stem Cell Biology and Regenerative Medicine FACS Core and the Neuroscience Microscopy Service (NMS) (NIH NS069375) for their technical support. This work was supported by the National Science Foundation (NSF) INSPIRE 1233054 (to O.J.A., A.Z., and E.K.), National Institutes of Health (NIH) (K01 HL130608) (to O.J.A.), NIH T32 Postdoctoral Fellowship (to E.T.), Austrian Science Fund (to J.R.), NIH K99 HL104002 (to I.K.), NIH R01 HL133272 (to J.C.W.), NIH R01 HL132875 (to J.C.W.), NIH R01 HL128170 and NIH R01 HL113006 and the California Institute for Regenerative Medicine (CIRM) (TR3-05556, RT3-07798, and DR2A-05394) (to J.C.W.), the German Research Foundation (DFG SFB 1002 [C04]) (to M.T.), as well as the DZHK (German Center for Cardiovascular Research), the German Federal

Ministry for Science and Education (BMBF FKZ 13GW0007A [CIRM-ETIII]), and the German Research Foundation (DFG SFB 1002 [C04, S01] and DFG SFB 937 [A18]) (to W.H.Z.).

Author Contributions

O.J.A.: conceived the study, oversaw, performed, analyzed, and interpreted all experiments, and wrote the manuscript, advised, performed, and oversaw cell culture, differentiation, and characterization, designed, created, and analyzed EHMs, and oversaw EHM experiments, performed and oversaw electrophysiology experiments, and analyzed and interpreted results, performed and oversaw immunocytochemistry and immunohistochemistry experiments, and analyzed and interpreted results, contributed to manuscript preparation; E.T.: conceived the study, oversaw, performed, analyzed, and interpreted all experiments, and wrote the manuscript, advised, performed, and oversaw cell culture, differentiation, and characterization, designed, created, and analyzed EHMs, and oversaw EHM experiments, performed and oversaw immunocytochemistry and immunohistochemistry experiments, and analyzed and interpreted results, contributed to manuscript preparation; H.Y.: advised, performed, and oversaw cell culture, differentiation, and characterization, designed, created, and analyzed EHMs, and oversaw EHM experiments, performed and oversaw immunocytochemistry and immunohistochemistry experiments, and analyzed and interpreted results, contributed to manuscript preparation; M.-T.Z., G.J., and D.B.: advised, performed, and oversaw gene expression experiments, and analyzed and interpreted results, contributed to manuscript preparation; A.M.Z. and E.K.: advised, performed, and oversaw computational model creation, and analyzed and interpreted results, contributed to manuscript preparation; M.T., I.K., and W.H.Z.: designed, created, and analyzed EHMs, and oversaw EHM experiments, contributed to manuscript preparation; J.R.: performed and oversaw immunocytochemistry and immunohistochemistry experiments, and analyzed and interpreted results, contributed to manuscript preparation; E.M., Y.Z., T.C., V.C.C., P.W.B., L.A.C., and J.D.G.: advised, performed, and oversaw cell culture, differentiation, and characterization, contributed to manuscript preparation; P.S.: performed and oversaw electrophysiology experiments, and analyzed and interpreted results, contributed to manuscript preparation; J.C.W.: conceived the study, oversaw, performed, analyzed, and interpreted all experiments, and wrote the manuscript, contributed to manuscript preparation.

Disclosure of Potential Conflicts of Interest

J.R. is an employee of Genentech. E.T. discloses an advisory role with Wilson Sonsini Goodrich and is an employee of Rosati. D.B. is a patent holder for RegenCor (collagen patch for cardiac regeneration). All other authors indicated no potential conflicts of interest.

References

1 Lloyd-Jones D, Adams RJ, Brown TM et al. Heart disease and stroke statistics–2010 update: A report from the American Heart Association. Circulation 2010;121:e46–e215.

2 Laflamme MA, Murry CE. Heart regeneration. Nature 2011;473:326–335.

3 Velagaleti RS, Pencina MJ, Murabito JM et al. Long-term trends in the incidence of heart failure after myocardial infarction. Circulation 2008;118:2057–2062.

4 Healy KE, McDevitt TC, Murphy WL et al. Engineering the emergence of stem cell therapeutics. Sci Transl Med 2013;5:207ed217.

5 Ye L, Zimmermann WH, Garry DJ et al. Patching the heart: Cardiac repair from within and outside. Circ Res 2013;113:922–932.

6 Thomson JA, Itskovitz-Eldor J, Shapiro SS et al. Embryonic stem cell lines derived from human blastocysts. Science 1998;282:1145–1147.

7 Takahashi K, Tanabe K, Ohnuki M et al. Induction of pluripotent stem cells from adult human fibroblasts by defined factors. Cell 2007;131:861–872.

8 Zhang J, Wilson GF, Soerens AG et al. Functional cardiomyocytes derived from human induced pluripotent stem cells. Circ Res 2009;104:e30–e41.

9 Lian X, Hsiao C, Wilson G et al. Robust cardiomyocyte differentiation from human pluripotent stem cells via temporal modulation of canonical Wnt signaling. Proc Natl Acad Sci USA 2012;109:E1848–E1857.

10 Burridge PW, Keller G, Gold JD et al. Production of de novo cardiomyocytes: Human pluripotent stem cell differentiation and direct reprogramming. Cell Stem Cell 2012;10:16–28.

11 Burridge PW, Matsa E, Shukla P et al. Chemically defined generation of human cardiomyocytes. Nat Methods 2014;11:855–860.

12 Caspi O, Lesman A, Basevitch Y et al. Tissue engineering of vascularized cardiac muscle from human embryonic stem cells. Circ Res 2007;100:263–272.

13 Stevens KR, Pabon L, Muskheli V et al. Scaffold-free human cardiac tissue patch created from embryonic stem cells. Tissue Eng Part A 2009;15:1211–1222.

14 Tulloch NL, Muskheli V, Razumova MV et al. Growth of engineered human myocardium with mechanical loading and vascular coculture. Circ Res 2011;109:47–59.

15 Shiba Y, Fernandes S, Zhu WZ et al. Human ES-cell-derived cardiomyocytes electrically couple and suppress arrhythmias in injured hearts. Nature 2012;489:322–325.

16 Chong JJ, Yang X, Don CW et al. Human embryonic-stem-cell-derived cardiomyocytes regenerate non-human primate hearts. Nature 2014;510:273–277.

17 Ye L, Chang YH, Xiong Q et al. Cardiac repair in a porcine model of acute myocardial infarction with human induced pluripotent stem cell-derived cardiovascular cells. Cell Stem Cell 2014;15:750–761.

18 Moretti A, Bellin M, Welling A et al. Patient-specific induced pluripotent stem-cell models for long-QT syndrome. New Engl J Med 2010;363:1397–1409.

19 Itzhaki I, Maizels L, Huber I et al. Modelling the long QT syndrome with induced pluripotent stem cells. Nature 2011;471:225–229.

20 Tiburcy M, Didie M, Boy O et al. Terminal differentiation, advanced organotypic maturation, and modeling of hypertrophic growth in engineered heart tissue. Circ Res 2011;109:1105–1114.

21 Yazawa M, Hsueh B, Jia X et al. Using induced pluripotent stem cells to investigate cardiac phenotypes in Timothy syndrome. Nature 2011;471:230–234.

22 Sun N, Yazawa M, Liu J et al. Patient-specific induced pluripotent stem cells as a model for familial dilated cardiomyopathy. Sci Transl Med 2012;4:130ra147.

23 Lan F, Lee AS, Liang P et al. Abnormal calcium handling properties underlie familial hypertrophic cardiomyopathy pathology in patient-specific induced pluripotent stem cells. Cell Stem Cell 2013;12:101–113.

24 McCain ML, Sheehy SP, Grosberg A et al. Recapitulating maladaptive, multiscale remodeling of failing myocardium on a chip. Proc Natl Acad Sci USA 2013;110:9770–9775.

25 Wang G, McCain ML, Yang L et al. Modeling the mitochondrial cardiomyopathy of Barth syndrome with induced pluripotent stem cell and heart-on-chip technologies. Nat Med 2014;20:616–623.

26 Liang P, Lan F, Lee AS et al. Drug screening using a library of human induced pluripotent stem cell-derived cardiomyocytes reveals disease-specific patterns of cardiotoxicity. Circulation 2013;127:1677–1691.

27 Braam SR, Tertoolen L, Casini S et al. Repolarization reserve determines drug responses in

human pluripotent stem cell derived cardiomyocytes. Stem Cell Res 2013;10:48–56.
28 Navarrete EG, Liang P, Lan F et al. Screening drug-induced arrhythmia [corrected] using human induced pluripotent stem cell-derived cardiomyocytes and low-impedance microelectrode arrays. Circulation 2013;128:S3–13.
29 Huebsch N, Loskill P, Deveshwar N et al. Miniaturized iPS-cell-derived cardiac muscles for physiologically relevant drug response analyses. Sci Rep 2016;6:24726.
30 Yang X, Pabon L, Murry CE. Engineering adolescence: Maturation of human pluripotent stem cell-derived cardiomyocytes. Circ Res 2014;114:511–523.
31 Karakikes I, Ameen M, Termglinchan V et al. Human induced pluripotent stem cell–derived cardiomyocytes. Circ Res 2015;117:80.
32 Myers FB, Silver JS, Zhuge Y et al. Robust pluripotent stem cell expansion and cardiomyocyte differentiation via geometric patterning. Integr Biol 2013;5:1495–1506.
33 Yang X, Rodriguez M, Pabon L et al. Triiodo-l-thyronine promotes the maturation of human cardiomyocytes-derived from induced pluripotent stem cells. J Mol Cell Cardiol 2014;72:296–304.
34 Nunes SS, Miklas JW, Liu J et al. Biowire: A platform for maturation of human pluripotent stem cell-derived cardiomyocytes. Nat Methods 2013;10:781–787.
35 Abilez OJ, Wong J, Prakash R et al. Multiscale computational models for optogenetic control of cardiac function. Biophys J 2011;101:1326–1334.
36 Soong PL, Tiburcy M, Zimmermann WH. Cardiac differentiation of human embryonic stem cells and their assembly into engineered heart muscle. In: Bonifacino JS, et al., eds. Current Protocols in Cell Biology. 2012; Chapter 23:Unit 23:28. John Wiley & Sons, Inc., Hoboken, NJ, USA.
37 Streckfuss-Bomeke K, Wolf F, Azizian A et al. Comparative study of human-induced pluripotent stem cells derived from bone marrow cells, hair keratinocytes, and skin fibroblasts. Eur Heart J 2013;34:2618–2629.
38 Thavandiran N, Dubois N, Mikryukov A et al. Design and formulation of functional pluripotent stem cell-derived cardiac microtissues. Proc Natl Acad Sci USA 2013;110:E4698–E4707.
39 Zhang D, Shadrin IY, Lam J et al. Tissue-engineered cardiac patch for advanced functional maturation of human ESC-derived cardiomyocytes. Biomaterials 2013;34:5813–5820.
40 Hirt MN, Boeddinghaus J, Mitchell A et al. Functional improvement and maturation of rat and human engineered heart tissue by chronic electrical stimulation. J Mol Cell Cardiol 2014;74:151–161.
41 Stoehr A, Neuber C, Baldauf C et al. Automated analysis of contractile force and Ca2+ transients in engineered heart tissue. Am J Physiol Heart Circ Physiol 2014;306:H1353–H1363.
42 Tiburcy M, Meyer T, Soong PL et al. Collagen-based engineered heart muscle. Methods Mol Biol 2014;1181:167–176.
43 Vollert I, Seiffert M, Bachmair J et al. In vitro perfusion of engineered heart tissue through endothelialized channels. Tissue Eng Part A 2014;20:854–863.
44 Tzatzalos E, Abilez OJ, Shukla P et al. Engineered heart tissues and induced pluripotent stem cells: Macro- and microstructures for disease modeling, drug screening, and translational studies. Adv Drug Deliv Rev 2016;96:234–244.
45 Chaturvedi RR, Herron T, Simmons R et al. Passive stiffness of myocardium from congenital heart disease and implications for diastole. Circulation 2010;121:979–988.
46 Ghista DN, Sandler H, Vayo WH. Elastic modulus of the human intact left ventricle–determination and physiological interpretation. Med Biol Eng 1975;13:151–161.
47 Granzier HL, Irving TC. Passive tension in cardiac muscle: Contribution of collagen, titin, microtubules, and intermediate filaments. Biophys J 1995;68:1027–1044.
48 Makarenko I, Opitz CA, Leake MC et al. Passive stiffness changes caused by upregulation of compliant titin isoforms in human dilated cardiomyopathy hearts. Circ Res 2004;95:708–716.
49 Kruger M, Kotter S, Grutzner A et al. Protein kinase G modulates human myocardial passive stiffness by phosphorylation of the titin springs. Circ Res 2008;104:87–94.
50 Yu J, Vodyanik MA, Smuga-Otto K et al. Induced pluripotent stem cell lines derived from human somatic cells. Science 2007;318:1917–1920.
51 Shukla P, Ghatta S, Dubey N et al. Maternal nutrient restriction during pregnancy impairs an endothelium-derived hyperpolarizing factor-like pathway in sheep fetal coronary arteries. Am J Physiol Heart Circ Physiol 2014;307:H134–H142.
52 Zimmermann WH, Fink C, Kralisch D et al. Three-dimensional engineered heart tissue from neonatal rat cardiac myocytes. Biotechnol Bioeng 2000;68:106–114.
53 Tiburcy M, Hudson JE, Balfanz P etet al. Defined engineered human myocardium with advanced maturation for applications in heart failure modelling and repair. Circulation 2017;
54 Yang L, Soonpaa MH, Adler ED et al. Human cardiovascular progenitor cells develop from a KDR+ embryonic-stem-cell-derived population. Nature 2008;453:524–528.
55 Urheim S, Rabben SI, Skulstad H et al. Regional myocardial work by strain Doppler echocardiography and LV pressure: A new method for quantifying myocardial function. Am J Physiol Heart Circ Physiol 2005;288:H2375–H2380.
56 Friedman C-E. A comparison of heart volume during life and after death. Acta Med Scand 1951;139:40–43.
57 Friedman C-E. Heart volume, myocardial volume and total capacity of the heart cavities in certain chronic heart diseases; a clinic, roentgenologic and patho-anatomic investigation of the problem of cardiac hypertrophy and dilatation and amount of residual blood of the heart. Acta Med Scand 1951;139:1–100.
58 Jung G, Fajardo G, Ribeiro AJ et al. Time-dependent evolution of functional vs. remodeling signaling in induced pluripotent stem cell-derived cardiomyocytes and induced maturation with biomechanical stimulation. FASEB J 2016;30:1464–1479.
59 Solaro RJ. Mechanisms of the Frank-Starling law of the heart: The beat goes on. Biophys J 2007;93:4095–4096.
60 Zimmermann WH, Melnychenko I, Wasmeier G et al. Engineered heart tissue grafts improve systolic and diastolic function in infarcted rat hearts. Nat Med 2006;12:452–458.
61 Radisic M, Park H, Shing H et al. Functional assembly of engineered myocardium by electrical stimulation of cardiac myocytes cultured on scaffolds. Proc Natl Acad Sci USA 2004;101:18129–18134.
62 Wei B, Jin JP. *TNNT1*, *TNNT2*, and *TNNT3*: Isoform genes, regulation, and structure-function relationships. Gene 2016;582:1–13.
63 Parton RG, Way M, Zorzi N et al. Caveolin-3 associates with developing T-tubules during muscle differentiation. J Cell Biol 1997;136:137–154.
64 Patel HH, Murray F, Insel PA. G-protein-coupled receptor-signaling components in membrane raft and caveolae microdomains. Handb Exp Pharmacol 2008;167–184.
65 Kane C, Couch L, Terracciano CM. Excitation-contraction coupling of human induced pluripotent stem cell-derived cardiomyocytes. Front Cell Dev Biol 2015;3:59.
66 Wang H, Svoronos AA, Boudou T et al. Necking and failure of constrained 3D microtissues induced by cellular tension. Proc Natl Acad Sci USA 2013;110:20923–20928.
67 Brandenburger M, Wenzel J, Bogdan R et al. Organotypic slice culture from human adult ventricular myocardium. Cardiovasc Res 2012;93:50–59.


See www.StemCells.com for supporting information available online.

